RESEARCH ARTICLE

Type IV Pilus Secretins Have Extracellular C Termini

Joshua A. Lieberman,[a] Courtney D. Petro,[b] Stefani Thomas,[c] Austin Yang,[d] Michael S. Donnenberg[a]

Department of Medicine, School of Medicine, University of Maryland, Baltimore, Maryland, USA[a]; Department of Biochemistry and Molecular Biology, School of Medicine, University of Maryland, Baltimore, Maryland, USA[b]; Department of Pathology, Johns Hopkins University, Baltimore, Maryland, USA[c]; Department of Anatomy and Neurobiology, School of Medicine, University of Maryland, Baltimore, Maryland, USA[d]

J.A.L. and C.D.P. contributed equally to this work.

ABSTRACT **Type IV pili (T4Ps) are surface appendages used by Gram-negative and Gram-positive pathogens for motility and attachment to epithelial surfaces. In Gram-negative bacteria, such as the important pediatric pathogen enteropathogenic *Escherichia coli* (EPEC), during extension and retraction, the pilus passes through an outer membrane (OM) pore formed by the multimeric secretin complex. The secretin is common to Gram-negative assemblies, including the related type 2 secretion (T2S) system and the type 3 secretion (T3S) system. The N termini of the secretin monomers are periplasmic and in some systems have been shown to mediate substrate specificity. In this study, we mapped the topology of BfpB, the T4P secretin from EPEC, using a combination of biochemical and biophysical techniques that allowed selective identification of periplasmic and extracellular residues. We applied rules based on solved atomic structures of outer membrane proteins (OMPs) to generate our topology model, combining the experimental results with secondary structure prediction algorithms and direct inspection of the primary sequence. Surprisingly, the C terminus of BfpB is extracellular, a result confirmed by flow cytometry for BfpB and a distantly related T4P secretin, PilQ, from *Pseudomonas aeruginosa*. Keeping with prior evidence, the C termini of two T2S secretins and one T3S secretin were not detected on the extracellular surface. On the basis of our data and structural constraints, we propose that BfpB forms a beta barrel with 16 transmembrane beta strands. We propose that the T4P secretins have a C-terminal segment that passes through the center of each monomer.**

IMPORTANCE **Secretins are multimeric proteins that allow the passage of secreted toxins and surface structures through the outer membranes (OMs) of Gram-negative bacteria. To date, there have been no atomic structures of the C-terminal region of a secretin, although electron microscopy (EM) structures of the complex are available. This work provides a detailed topology prediction of the membrane-spanning domain of a type IV pilus (T4P) secretin. Our study used innovative techniques to provide new and comprehensive information on secretin topology, highlighting similarities and differences among secretin subfamilies. Additionally, the techniques used in this study may prove useful for the study of other OM proteins.**

Received 2 March 2015 **Accepted** 4 March 2015 **Published** 24 March 2015

Citation Lieberman JA, Petro CD, Thomas S, Yang A, Donnenberg MS. 2015. Type IV pilus secretins have extracellular C termini. mBio 6(2):e00322-15. doi:10.1128/mBio.00322-15.

Editor Philippe J. Sansonetti, Pasteur Institute

Address correspondence to Michael S. Donnenberg, mdonnenb@medicine.umaryland.edu.

This article is a direct contribution from a Fellow of the American Academy of Microbiology.

Type IV pili (T4Ps) are long nanofibers comprised of subunits of the pilin structural protein (1, 2). T4Ps are the only class of pili found in both Gram-negative and Gram-positive bacteria as well as archaea (3–5). Many important bacterial pathogens express a T4P system, including *Clostridium difficile* (6), *Pseudomonas aeruginosa* (7, 8), *Neisseria gonorrhoeae* (9), *Vibrio cholerae* (10), and enteropathogenic *Escherichia coli* (EPEC) (11). EPEC is an important cause of infectious diarrhea in young children, particularly affecting infants in Africa, and is associated with fatal outcomes (12).

T4Ps can be further divided into T4aPs and T4bPs based on genetic organization of the genes responsible for expression and differences in the pilin protein. While the genetic components of T4bPs are organized in operons and the prepilin proteins have long leader sequences, T4aPs are encoded by unlinked loci and their pilin proteins are smaller and simpler in structure. T4bPs are common to enteric bacteria (1, 2). EPEC produce a prototypical T4bP called the bundle-forming pilus (BFP). The BFP mediates initial attachment to the intestinal epithelium and is a confirmed virulence factor (13). BFP expression is also associated with autoaggregate formation in liquid media and clustering when incubated with eukaryotic cells, a pattern known as "localized adherence" (14, 15).

A complex of 10 to 18 proteins is responsible for assembly and disassembly of T4Ps. In Gram-negative bacteria, the T4P biogenesis machine spans both the inner membrane (IM) and the outer membrane (OM) (16–18). The T4P is anchored in the IM and is extended and retracted through the OM secretin (19). Secretins serve a similar function in the type 2 secretion (T2S) and type 3 secretion (T3S) systems and filamentous bacteriophages (1, 20–23). In the T3S system, the secretin permits a molecular needle to protrude through the OM to inject virulence factors into host

cells. In T2S systems, soluble proteins, including toxins, are secreted directly into the extracellular milieu through the secretin protein (23–25). In each case, the secretin pore is strictly required for passage of large substrates through the OM.

Secretins form homomultimers of 12 to 15 monomers, and several ultrastructures have been solved by electron microscopy (EM) (24, 26–29). The EM structures reveal partially gated pores approximately 50 to 100 Å in diameter. All secretins are comprised of a large periplasmic vestibule and a C-terminal domain rich in predicted beta strands. Multiple conformations for the secretin pore are likely required to permit substrate transport; at least some of these conformations have been observed directly (19) or inferred (25, 29). Finally, in almost all cases, rotational symmetry has been observed. While 12-fold rotational symmetry appears to be the most common, 14-fold and 15-fold symmetry have also been observed (24, 30, 31). Interestingly, one report identified a strong 4-fold rotational symmetry, suggesting a "tetramer of trimers" for the PilQ secretin of *Neisseria meningitidis* (32), while the closely related protein from *N. gonorrhoeae* is composed of 14 monomers (33). It therefore seems likely that different secretin-utilizing systems display variations in the architecture of this pore complex, while retaining core features.

More-detailed structures of secretin molecules, either monomers or complexes, have remained elusive. The multimer is too large to resolve by nuclear magnetic resonance (NMR), and membrane proteins are notoriously difficult to crystallize due to the detergents required to solubilize the proteins from their native state. Recently solved crystal structures of the periplasmic N termini of three secretin molecules have revealed conserved features that appear to underlie substrate transport, despite the considerable variability of secretin N termini across the superfamily. The N-terminal structures of GspD, the T2S secretin of enterotoxigenic *E. coli* (34), of EscC, the secretin of the EPEC T3S apparatus (35), and HofQ, the secretin of the *Aggregatibacter actinomycetemcomitans* required for DNA uptake (36), exhibit several domains within the N terminus.

In contrast to the progress made defining the atomic structures of the N termini of secretins and the pore ultrastructure, little progress has been made toward understanding the structure of the C-terminal "secretin domain" (Pfam structural domain 00263; Pfam database [http://pfam.sanger.ac.uk/]) presumed to form a beta barrel in the OM. In lieu of atomic data, several attempts have been made to map the topology of secretin molecules through a combination of *in silico* prediction methods, biochemical labeling coupled with observation by EM (26, 37), mutational analysis to identify the gating domains (38), and sites of protease sensitivity (39). These studies have produced topology models with various numbers of transmembrane strands, and each is fraught with uncertainties.

The topology models for XcpQ (*P. aeruginosa*, T2S) and PilQ (*N. meningitidis*, T4aP) predicted 13 transmembrane beta strands (TMBSs) (26, 37), while the pIV protein of the *E. coli* filamentous phage assembly was predicted to have 11 TMBSs (38). The predicted odd number of TMBSs in all three cases is quite striking; to date, all known bacterial OM beta barrels have an even number of beta strands (40–42).

Almost all studies of secretins thus far have assumed that these proteins span the OM as a transmembrane beta barrel for two reasons. With very few exceptions, OM proteins form beta barrels, all of which have an even number of beta strands (41–43). Furthermore, secretins have been predicted to be rich in beta strands, particularly in the C-terminal secretin domain (24, 44).

Solved structures of OM beta barrels have consistently contained 8, 10, 12, 16, 18, 22, 24, or 26 antiparallel beta strands. The strands consist of at least 6, but more commonly 8 to 11 amino acids, with short periplasmic turns of 1 to 8 residues, and variable extracellular loops that may be longer than 50 amino acids (42, 45–51). Barrel diameters for each pore type correspond approximately to the number of beta strands and are on the order of 20 to 25 Å for 8- and 12-stranded barrels (45, 47), 30 to 35 Å for 16-stranded barrels (48), and as large as 35 to 50 Å for the 22-stranded barrels (49–51). Most of these outer membrane proteins (OMPs) exist as monomers with an elliptical cross section, although known 16-stranded porins form homotrimers (45, 47–51).

Other structures that allow proteins to span the OM have been identified; two of these structures are variations on the theme of a beta barrel with an even number of membrane-spanning segments. Classical autotransporter (AT) proteins, such as NalP of *N. meningitidis* (52), consist of an N-terminal passenger domain which is transported through the pore of a beta barrel with an even number of beta strands formed by the C terminus (47, 53). The EPEC adherence factor intimin (54) is a type 5e AT protein with an inverse structure relative to the classical AT: the C terminus of intimin is transported across the OM by an N-terminal beta barrel domain (55). Alternatively, OM beta barrels may be assembled from multiple protomers, usually a trimer as in the type 1 secretion (T1S or Tol) system; each protomer donates three strands to the antiparallel beta barrel (56, 57). Recently, two radically different complexes of OM-spanning proteins have been identified. The octomeric polysaccharide transporter Wza (58) and VirB10 of the type IV secretion system (59) consist of alpha helices wrapped in a "beta sandwich" conformation and embedded in both the IM and OM.

In the absence of atomic level data, resolving the fine topology of BfpB is a key step in understanding the architecture of the BFP and other T4P biogenesis machines, as well as the general structure of all secretins. To generate a model topology of BfpB, we combined multiple novel biochemical and biophysical assays with secondary structure analysis from several algorithms and utilized known features of OMP beta barrels to guide assignment of transmembrane beta strands. We tested our model with representative secretins from the T4aP, T2S, and T3S systems.

RESULTS

Iodination mass spectrometry to guide BfpB topology modeling. As a screening tool to identify solvent-exposed tyrosine and histidine residues, we used nonradioactive iodinate as a mass label for mass spectrometry and proteomic detection. We iodinated purified BfpB using a catalyst immobilized in the lumen of glass tubes (Iodogen tubes) (catalog no. 28601; Pierce). We identified eight iodinated residues in purified protein (Table 1). Four of these were in the proximal 171 amino acids previously identified as the BfpB periplasmic domain (34, 60).

To identify extracellular tyrosine residues, we next iodinated intact cells expressing BfpB and then purified BfpB before performing mass spectrometry and proteomic identification. Previous experiments with radioactive iodine have been used to successfully identify surface-exposed residues (61–63). We hypothesized that the four proximal residues (H37, Y64, H86, and H116) would not be identified if we iodinated whole cells, since

TABLE 1 All iodinated residues identified by LC-MS/MS

Residue	Iodinated residue identified in purified protein[a]
H37	3/9
H50	
Y51	
Y64	1/1
H86	1/12
H116	1/1
Y184	
Y215	
Y272	3/6
Y296	1/4
Y315	
Y360	1/1
Y503	3/8

[a] Data are presented as number of peptide spectrum matches (PSMs) with an iodinated residue over all PSMs containing that residue.

catalyst is immobilized on glass tubes, and the reactivity of the short-lived iodous (I^+) intermediate is limited by diffusion. Four residues (Y215, Y315, Y360, and Y503) were iodinated ≥5% of the time and were identified with high probability (number of sibling peptides [NSP] adjusted probability score; see Table S1 in the supplemental material), indicating that they are likely extracellular. Two residues (Y184 and Y296) were iodinated ≤5% of the time they were identified. In addition, two residues in the known periplasmic domain (H50 and Y51) were identified as iodinated in a single peptide spectrum match (PSM) with a low probability score in a double-labeled peptide (Fig. 1 and Table S1). Representative spectra are shown in Fig. S1 in the supplemental material, and a complete list of identified peptides is provided in Table S1.

Sulfhydryl labeling of site-directed cysteine mutations reveals solvent accessibility. We hypothesized that the distal residues identified by intact cell iodination were likely extracellular and that the proximal four residues iodinated by labeling purified protein were periplasmic. To test this hypothesis, we made site-directed mutations of the plasmid encoding streptavidin (Strep)-tagged BfpB changing serine or threonine residues to cysteines for labeling with sulfhydryl-selective reagents. Wild-type BfpB contains two endogenous cysteines, C18 and C539. C18 is the target of palmitoylation by the Lol pathway (64, 65). Its sulfhydryl group is involved in a thioether bond with diacylglycerol and buried in the inner leaflet of the OM and is thus unavailable to react with sulfhydryl-labeling reagents. Multiple *in silica* models of BfpB topology predict C539 to be buried in a TMBS (see Fig. S2 in the supplemental material). On the basis of the results of the iodination experiments, we constructed an initial panel of 16 BfpB-cysteine scanning mutants (BfpB-CSMs [Table S2]) plus a $BfpB_{C539S}$ "cysteine-free" negative control. To minimize biochemical alterations, we targeted serine residues, as they differ from cysteine in only a single atom, and the highly similar threonine residues.

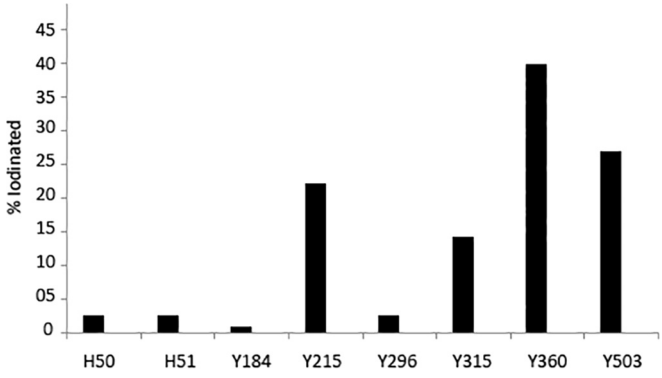

FIG 1 Iodination of extracellular residues in intact cells. Purified BfpB from labeled intact cells was subjected to MS identification of extracellular residues as indicated by an iodination event. The graph displays the number of iodination events divided by the total number of times the peptide was recovered to yield an iodination percentage.

Two important control cysteine mutations were made. $BfpB_{T309C}$ was selected as an extracellular control, because T309 is close to Y315, which was labeled with iodine in intact cells. Furthermore, Y296, which was also labeled, albeit with low efficiency, might also be extracellular, in which case T309 must also be outside. $BfpB_{S41C}$ was made as a periplasmic control, because S41C lies within the periplasmic N-terminal domain between H37 and Y64, both of which were iodinated exclusively when purified BfpB was the substrate. The remaining mutations were made in regions of the primary sequence the topology of which was not elucidated by the iodination experiments.

Two of the 16 point mutations, $BfpB_{S198C}$ and $BfpB_{S462C}$, did not produce stable protein as assessed by Western blotting, while four produced stable proteins that could not restore autoaggregation to the *bfpB* null mutant UMD923 by complementation in *trans* and were therefore nonfunctional (see Table S2 in the supplemental material). The remaining 11 constructs, including $BfpB_{C539S}$, were tested along with wild-type BfpB for solvent accessibility by *in situ* labeling with the sulfhydryl-reactive trimethyl maleimide polyethylene glycol [$TMM(PEG)_{12}$]. Wild-type BfpB, $BfpB_{S490C}$, and the negative-control $BfpB_{C539S}$ were never labeled, while the periplasmic control $BfpB_{S41C}$ labeled weakly; all other constructs labeled consistently with $TMM(PEG)_{12}$ (Fig. 2). These results indicate that all targeted residues except C490 and C539 are solvent accessible. Furthermore, labeling of C41 indicates that $TMM(PEG)_{12}$ is able to cross the OM.

***In vitro* FRET determines the orientation of cysteine mutations to the OM.** To determine whether each mutated cysteine residue is extracellular or intracellular, we measured intramolecular Förster resonance energy transfer (FRET) on purified BfpB-Strep complexes, using streptavidin Alexa Fluor 488 (SA-488) as the donor fluorophore and the panel of Bfp-CSM constructs conjugated to tetramethylrhodamine-C5-(and-C6)-C2-maleimide (TAMRA-maleimide) as the FRET receptor.

We hypothesized that FRET would occur in double-labeled proteins between the C-terminal streptavidin labeled with SA-488 and the periplasmic S41C conjugated to TAMRA-maleimide, but not between the C terminus and the T309C extracellular control, as all secretins are thought to be OM beta barrels (24), and all known OM beta barrels have an even number of TMBSs (41, 42). Surprisingly, we found the opposite to be the case. FRET occurred between the labeled C terminus and the extracellular residue T309C, but no FRET occurred when the periplasmic S41C residue was labeled (Fig. 3). The wild-type protein containing an endogenous cysteine at C539, which was not solvent accessible in $TMM(PEG)_{12}$ labeling experiments, displayed 9% (±4%) FRET efficiency.

We tested the remaining cysteine point mutations for their ability to FRET with the labeled C terminus. We also constructed

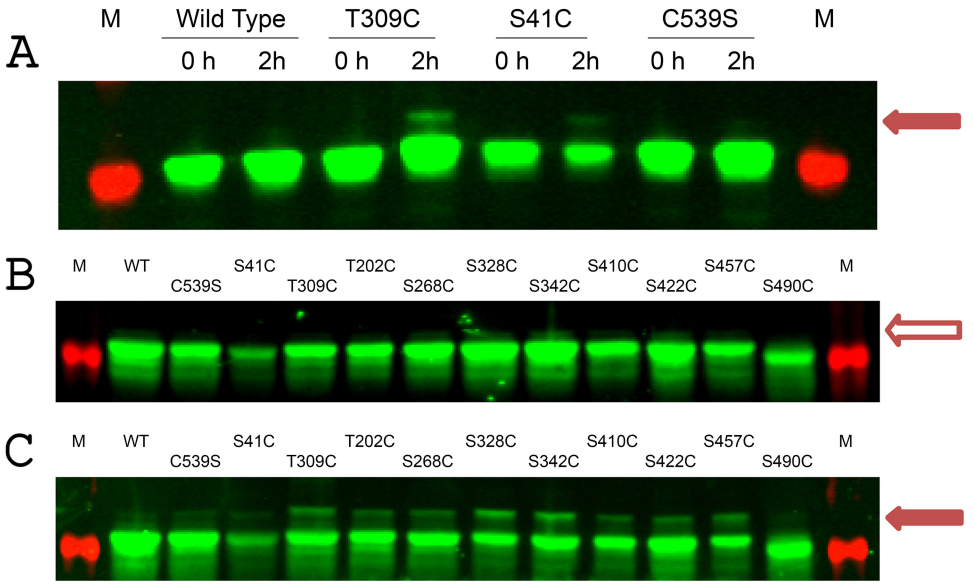

FIG 2 Solvent accessibility labeling of BfpB-CSM. Western blot results from TMM(PEG)$_{12}$ labeling of BfpB-CSM. The 50-kDa marker bands are shown in lanes M. (A) Results of TMM(PEG)$_{12}$ labeling of control BfpB-CSM constructs. After 2-h incubation with the reagent, a second band (solid arrow) with decreased M_r was observed, indicating that a positive label was consistently observed for BfpB$_{T309C}$ and BfpB$_{S41C}$. No such band was ever observed with either wild-type (WT) BfpB or BfpB$_{C539S}$. (B) Control to confirm that the slower-migrating band is due to TMM(PEG)$_{12}$. The Western blot shows the absence of the slower-migrating band without TMM(PEG)$_{12}$ labeling (open arrow). (C) TMM(PEG)$_{12}$ labeling of all BfpB-CSM mutants reveals that all but three (wild-type BfpB, BfpB$_{C539S}$, and BfpB$_{S490C}$) are labeled and therefore solvent accessible.

a "maximal FRET" control cysteine mutation in the 2-amino-acid linker region between the BfpB primary sequence and the streptavidin binding affinity tag, creating BfpB$_{S553C}$, and used the protein lacking the native C539 residue, BfpB$_{C539S}$, as a null FRET control. The BfpB$_{S553C}$ positive control had a FRET efficiency of 49% (±11%), while the BfpB$_{C539S}$ negative control was not statistically different from the wild type (1% and 0.7%, respectively). In addition to BfpB$_{T309C}$, only two BfpB residues permitted energy transfer from the C-terminal label, S422C and S457C (Fig. 3). FRET acceptor labeling was confirmed by robust TAMRA fluorescence emission in each of the BfpB-CSM constructs except BfpB$_{C539S}$. Curiously, S490C was labeled by TAMRA-maleimide at levels similar to that of the wild type despite not being labeled by TMM(PEG)$_{12}$, although no FRET was observed in either the S490C or C539S constructs. Estimates of the efficiency of labeling BfpB molecules in the FRET experiments were performed by comparing BfpB-CSM acceptor fluorescence emission with a standard curve of emission intensities using known concentrations of TAMRA-maleimide-labeled BfpB (see Table S2 in the supplemental material).

Flow cytometry confirms that T4P secretins have extracellular C termini, while other secretins do not. Given the surprising result of our *in vitro* FRET experiments, we tested the hypothesis that the C terminus of BfpB is extracellular by performing flow cytometry on intact cells expressing wild-type BfpB-Strep labeled with SA-488. For controls, we cloned genes for the periplasmic DsbA protein and the OM protein intimin truncated at residue 557 into the same pASK-IBA3 Strep expression vector. The C terminus of intimin extends through the pore of the OM beta barrel, and residue 557 is predicted to fall 7 amino acids beyond the OM based on the crystal structure of intimin (54). Thus, we utilized intimin$_{557}$ as a positive-control OM protein with a short extracellular C terminus. We also cloned the following genes into pASK-IBA3: *pilQ*, which codes for the T4aP secretin of *P. aeruginosa*; *escC*, the T3S secretin from EPEC; *gspD*, the T2S secretin from *E. coli*; and *epsD*, the T2S secretin from *V. cholerae*. The T3S and T2S secretins require a pilotin to localize to the OM, and their C termini are known to interact with pilotin in the periplasm.

Flow cytometry on cells expressing these constructs labeled with SA-488 revealed two distinct classes of secretins (Fig. 4). The percentage of positive cells expressing either BfpB or PilQ labeled with SA-488 was similar to that of the positive control, intimin$_{557}$. In contrast, a very low percentage of positive cells was observed for DsbA labeled with SA-488. The percentages of positive cells for EscC, EpsD, and GspD, secretins from T3S and T2S systems, labeled with SA-488 were all similar to that for the negative control, DsbA.

The distal C terminus of BfpB reduces cell permeability but is dispensable for BFP function. To account for the finding that the C-terminal tag of BfpB is exposed to the extracellular environment while preserving an even number of transmembrane (TM) beta strands, we hypothesized that the last 16 residues of BfpB form an intrapore segment (IPS) allowing the tag to pass through the pore of each BfpB monomer. We further hypothesized that this structure-function relationship prevents entry of small molecules through the OM. We therefore constructed two C-terminal deletion mutants of BfpB: in BfpBΔIPS, the distal 16 residues were deleted, while in BfpBΔTMBS$_{16}$, the distal 42 residues were deleted. BfpBΔIPS robustly complemented the *bfpB* mutant UMD923 and produced stable protein detected on Western blots, while BfpBΔTMBS$_{16}$ did neither of these (see Fig. S3A in the supplemental material). We then performed flow cytometry on cells expressing BfpBΔIPS with a C-terminal Strep tag. Unlike the wild-type BfpB, the deletion mutant was not significantly different from the negative control (Fig. 4). We engineered the S41C and T309C mutations in BfpBΔIPS and prepared BfpBΔIPS with and

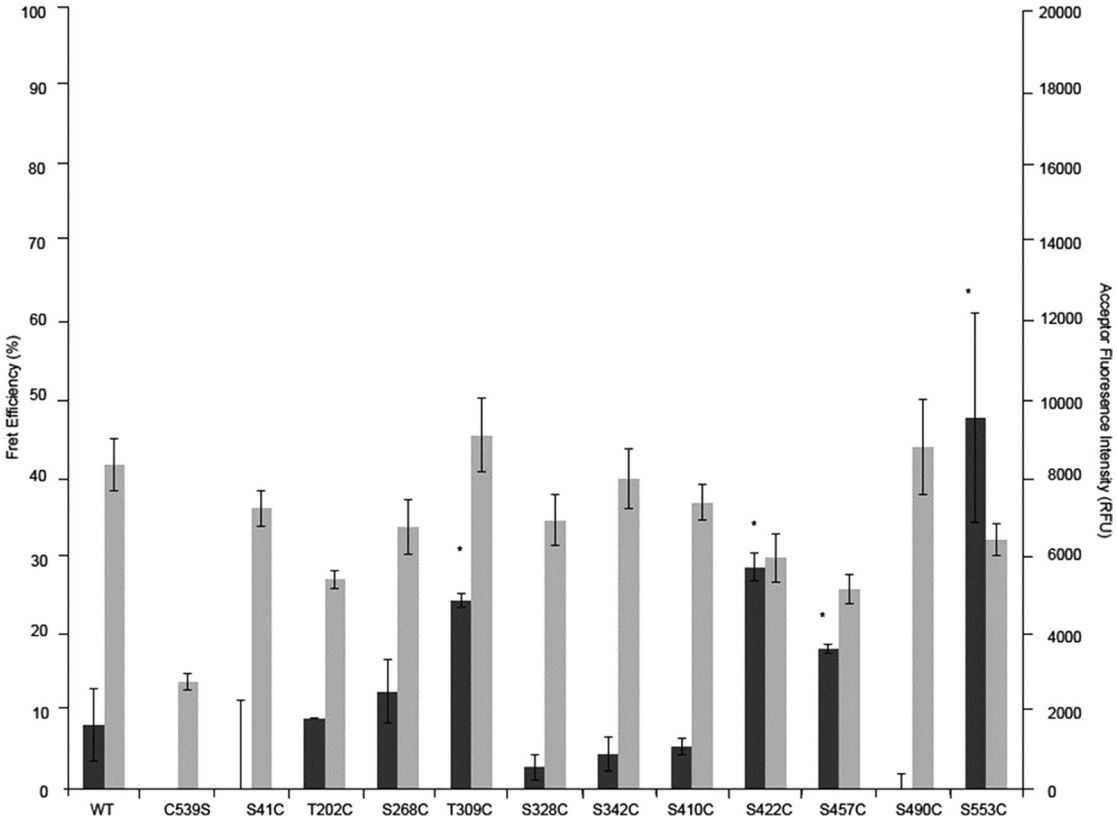

FIG 3 Förster resonance energy transfer (FRET) following *in vitro* labeling of BfpB cysteine mutants. The engineered and single endogenous cysteine residues in BfpB were labeled with TAMRA-maleimide, and the BfpB C terminus was labeled with streptavidin-Alexa Fluor 488. For each construct, FRET efficiency (as a percentage) was calculated from three independent labeling experiments. The primary *y* axis (left) shows FRET efficiency (black bars), while the secondary *y* axis (right) shows acceptor fluorescence (in arbitrary units; RFU, relative fluorescence units) (gray bars). Error bars show standard deviations. Asterisks indicate FRET signals significantly different from the wild-type BfpB baseline, as determined by ANOVA.

without cysteine mutations for FRET. However, all three proteins completely degraded during purification, and therefore, we were unable to perform the experiment.

We tested the hypothesis that the IPS provides resistance to cell permeability by measuring the rate of ampicillin consumption in cells expressing the pASK-IBA3 vector, wild-type BfpB, or BfpBΔIPS. We reasoned that an increased rate of ampicillin consumption indicated increased permeability, because the beta-lactamase protein Bla is found in the periplasm (66). Indeed, we found that ampicillin was consumed at a significantly higher rate by cells expressing BfpBΔIPS than by those expressing wild-type BfpB or no BfpB (see Fig. S3B in the supplemental material).

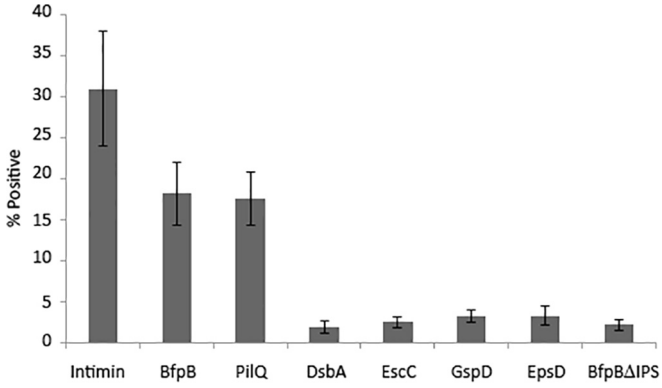

FIG 4 Flow cytometry of BfpB and PilQ *in situ* reveals an extracellular C terminus for T4P secretins. Cells expressing either DsbA (negative control), intimin$_{557}$ (positive control), BfpB, PilQ (*P. aeruginosa*, T4P), EscC (EPEC, T3S), GspD (enterotoxigenic *E. coli*, T2S), EpsD (*V. cholerae*, T2S), or BfpBΔIPS, each with an N-terminal Strep tag, were labeled with SA-488 in triplicate experiments and analyzed by flow cytometry for surface fluorescence. Results are expressed as a percentage of positive cells for each sample.

An alignment of sequences representing secretins in the T4aP, T4bP, T2S, and T3S families was constructed to analyze the IPS region for significant differences among secretins for each family and for similarities between T4aP and T4bP secretins. However, we were not able to identify patterns in protein sequences in the C termini that distinguished the secretin family types (not shown).

DISCUSSION

We have demonstrated a novel topology for T4P secretins in which the distal C-terminal fragment is exposed to the extracellular environment. We propose that this fragment passes through the central channel of the monomer from which it emanates. Furthermore, we generated a model topology of BfpB with 16 transmembrane beta strands. For details of the rationale underlying selection of each TMBS, please see supplemental material. Our prediction is based primarily on the novel biochemical and biophysical methods described above, cou-

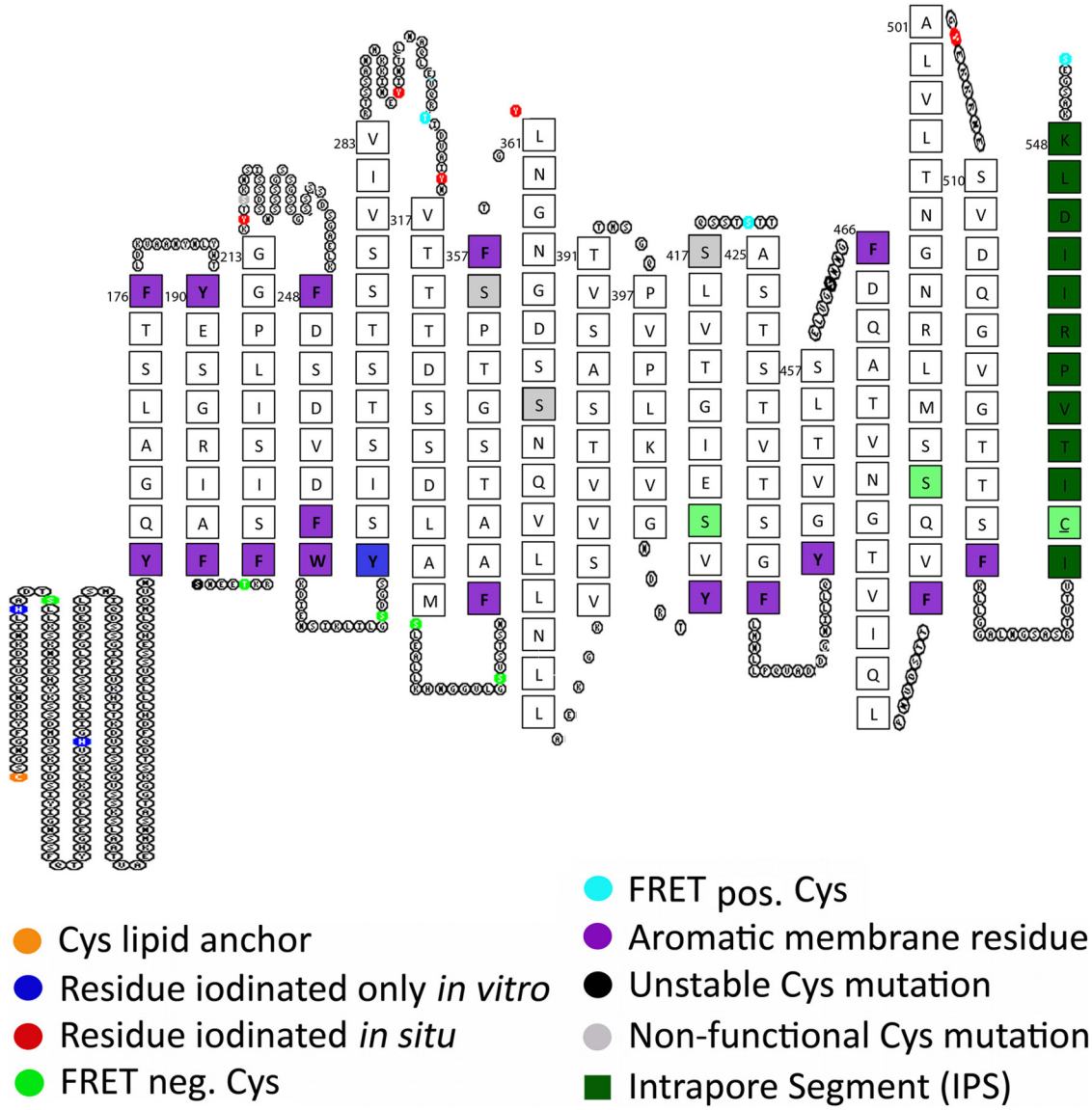

FIG 5 Model topology of BfpB with 16 transmembrane beta strands and an intrapore segment. The predicted topology of BfpB is presented here from the N terminus to the C terminus with the extracellular space at the top of the page and the periplasmic space at the bottom, generated in part using the TOPO2 program (S. J. Johns, TOPO2 transmembrane protein display software [http://www.sacs.ucsf.edu/TOPO2/]). The N-terminal, lipid-anchored cysteine, C18, is colored gold. Tyrosines and histidines labeled exclusively by iodination of purified protein are colored blue, while residues iodinated in intact cells are colored red. Residues that were mutated to cysteines and utilized for FRET experiments, as well as the endogenous C539, are colored by FRET labeling results: light green if FRET negative (neg.) or cyan if FRET positive (pos.). Residues colored black indicate that a cysteine mutation resulted in an unstable BfpB protein, while residues colored gray indicate that a cysteine mutation produced stable BfpB multimers but did not complement the *bfpB* mutant for autoaggregation. Aromatic residues are colored magenta. The 16th strand contains a putative *E. coli* Bam-stop signal, consisting of a terminal Phe (98). Beyond the 16th strand is the intrapore segment (IPS), which is predicted to extend from I538 to K548.

pled with multiple predictions of secondary structure and direct inspection of the primary sequence (Fig. 5; see Table S3 in the supplemental material).

Prior to this study, only a few topology models of secretin structures had been proposed, and these models were based almost entirely on secondary structure predictions (26, 29, 37, 67). The current model represents a substantial advance on these predictions, since the paucity of OMP sequence homology limits the accuracy of TMBS prediction (68, 69). Further, other OMP topology predictions have tended to overestimate the number of transmembrane beta strands: the iron transporter FhuA was predicted to have 32 strands (70), while the crystal structure revealed 22 strands (51); extensive mutagenesis studies of PapC led to 26 predicted strands (71), while the crystal structure revealed 24 strands (72, 73).

Our *a priori* assumption was that BfpB formed a typical OMP beta barrel, and thus, we required that (i) the predicted topology model contained an even number of TMBSs and that (ii) putative beta strands contain at least 6 amino acids. Finally, we assumed that the N terminus of BfpB was periplasmic, in agreement with crystal structures of the N termini of secretins (35, 74) and biochemical data demonstrating that the N termini of secretins inter-

act with periplasmic proteins within their respective secretion systems (25, 60, 75).

Differentiating periplasmic and extracellular residues is not a trivial task, as the OM is a molecular sieve with permeability restricted based on molecular shape, size, and charge (76, 77 this study). Furthermore, the BfpB multimer itself is sufficient to confer permeability to vancomycin (molecular mass of 1.485 kDa, PubChem ID 14970) (78). Although we could label solvent-exposed cysteine residues with the 2.3-kDa sulfhydryl-reactive $TMM(PEG)_{12}$ compound, we labeled both our periplasmic and extracellular control cysteine point mutations (S41C and T309C, respectively), and the labeling efficiency did not correlate with subsequent predictions regarding periplasmic or extracellular location (Fig. 2). Thus, despite its size, labeling with $TMM(PEG)_{12}$ could not distinguish between extracellular and periplasmic proteins. Unlike $TMM(PEG)_{12}$-maleimide, TAMRA-maleimide was likely able to access the S491C residue by virtue of its smaller size (553 Da).

We used iodination-mass spectrometry to guide placement of cysteine point mutations. Solvent-accessible residues were identified by $TMM(PEG)_{12}$-maleimide labeling. We probed the topology of the point mutants by FRET (Fig. 3) using TAMRA-maleimide as the cysteine-reactive moiety bearing an acceptor fluorophore and a donor fluorophore-coated streptavidin protein (SA-488) that would bind the C-terminal affinity tag.

We reasoned that since the streptavidin tetramer is 54 by 58 by 48 Å (79), while the thickness of the OM in *E. coli* is approximately 6 to 7 nm (80), the distance between donor and acceptor fluorophores if separated across the OM would be >7.5 nm. Since FRET efficiency is highly dependent on distance (a function of the inverse sixth power), with essentially no energy transfer predicted to occur at 10 nm and a steep efficiency curve (81), we predicted very low efficiency FRET across the OM. Previously we reported that the BfpB dodecameric complex has a maximum external diameter of 20 nm (65), suggesting a maximum distance of 5.2 nm between the centers of neighboring monomers. Given the width of streptavidin, we predicted highly efficient FRET between acceptor-labeled cysteine residues on the same side of the membrane as the donor fluorophore. We did not assign distance estimates based on the FRET results given the difficulties in establishing the κ factor upon which these estimates critically depend (81–83).

The flow cytometry results strongly support an extracellular topology for the C terminus of BfpB, as this labeling was similar to that of cells expressing the intimin protein truncated in a known extracellular domain (54) and was consistently different from that of the negative control. The substantially lower percentage of positive cells expressing the negative control, the periplasmic DsbA protein, confirms that the large streptavidin protein cannot cross the OM.

To account for our finding that the C terminus is extracellular without violating our initial assumptions drawn from typical OMPs, we propose that the distal C terminus of BfpB extends through either (i) the pore of an individual BfpB monomer or (ii) the central channel formed by the BfpB multimer. We suggest that the former is more likely, since the channel would have to accommodate 12 such segments, which would be likely to inhibit translocation of the pilus. Additionally, there is precedent for an IPS as analogous to the C terminus of intimin (55) or in the opposite configuration relative to the beta barrel, the passenger domains of AT proteins (47).

We predicted that the IPS extends from I538 to K548 (Fig. 5), since the endogenous cysteine residue C539 did not label with $TMM(PEG)_{12}$ and gave minimal baseline FRET in wild-type BfpB labeled with acceptor and donor fluorophores. We therefore concluded that C539 was probably in the monomer pore itself, inaccessible to $TMM(PEG)_{12}$, and near the periplasmic leaflet of the OM to account for the minimal FRET. This strand contains a mixture of polar and nonpolar residues, including one positively charged residue (R543) and one negatively charged residue (D546) that could help stabilize polar residues in the TMBSs (Fig. 5).

Our flow cytometry data demonstrate that the extracellular location of the C terminus is not a feature unique to BfpB but that this arrangement is also found in the T4aP secretin PilQ of *P. aeruginosa*. Unsurprisingly, this feature was not consistent among all secretins tested: T3S and T2S secretins bearing a streptavidin binding peptide affinity tag did not demonstrate fluorescence greater than that of the negative control. These secretins have periplasmic C termini (34, 35, 84). They also require pilotin proteins to localize to the OM and thus further validate the assay (85, 86). Curiously, we did not identify clear features in C-terminal sequences that could distinguish T4P secretins from T2S or T3S secretins. PilQ appears to tolerate deletion of the most distal 8 amino acids (707 to 714) without adversely affecting function or stability (87). Similarly, we were able to delete the IPS from BfpB without a gross adverse impact on function. In contrast, as predicted from our 16 TM beta strand model, deletion of the proposed 16th strand rendered the protein too unstable to be detected by immunoblotting. Notably, the BfpBΔIPS protein was stable *in vivo*, but its expression permitted increased ampicillin influx, as predicted by our model in which this region plugs the pore in each monomer.

The topology model we have generated suggests 16 transmembrane beta strands. Previous electron microscopy studies of secretins have suggested a wall thickness between 2 and 4.8 nm, which would correspond roughly to the external diameter of a secretin beta barrel monomer. This size corresponds well with either the 12- or 16-stranded OMPs. The 16-stranded beta barrels, as with most OMPs, have an elliptical cross section. The external diameters of these proteins are in the range of 4.0 nm with a short axis length around 3.0 nm (46, 48, 88–90). The 12-stranded beta barrels generally have external diameters less than 3.0 nm (47, 52, 56, 57). The single 10-stranded beta barrel we identified in our review of the literature, OmpT, has an external diameter of 3.2 nm (91). From our previously published electron microscopy data, we estimate a wall thickness for BfpB of about 3 nm (65) (unpublished data), a value that is consistent with the commonly identified OM beta barrel structure of 16 TMBSs.

Using all available experimental data, coupled with secondary structure predictions, direct analysis of primary amino acid sequence, and previously reported diameters of secretins, we propose that the topology of BfpB comprises 16 beta strands. Another alternative taking into account strictly experimental data suggests that a 14-stranded topology is possible. Because iodination of Y184 in intact cells occurred only 0.5% of the time we identified the peptide, a value similar to that observed for known periplasmic residues, this residue could potentially be periplasmic. This alternative would place predicted beta strands one and two in the periplasm. Additionally, FRET experiments indicate that T202 is periplasmic. The first residue for which there is strong evidence of

an extracellular location is Y215, which was iodinated 22% of the time that we identified the peptide. Thus, if Y184 is periplasmic, the first beta strand would start at F205. The remaining 13 beta strands would follow as they do for the 16-strand model.

We present the most robust topology mapping of a secretin beta barrel domain thus far, having relied on a multimodal approach that combined several biochemical labeling methods, biophysical measurements, multiple secondary structure predictions, direct inspection of the primary sequence, and the compatibility of our model with structural data available for both secretins and solved OMPs. However, our topology model of BfpB raises more questions about the structure of these unique OMP multimeric complexes than the model answers. Do all secretins have 16 (or 14) transmembrane beta strands? How different are the T2S, T3S, and T4P secretins? Are these proteins beta barrels at all, or do they adopt an uncommon structure? To date, only two OMPs have been characterized that do not form beta barrels, the octameric polysaccharide transporter Wza (58) and VirB10 of the type IV secretion system (59). Until a secretin structure is solved at the atomic level, these questions will remain unanswered.

MATERIALS AND METHODS

Strains, plasmids, and growth conditions. All strains and plasmids used in this study are presented in Table S4 in the supplemental material. Bacterial strains were cultured in Luria-Bertani (LB) broth at 37°C. In EPEC strains, BFP was expressed as previously described (92), by growing strains in Dulbecco's modified Eagle medium (DMEM) lacking phenol red. Antibiotics (ampicillin, 200 μg ml^{-1}; kanamycin 50 μg ml^{-1}) were added to select for or maintain plasmids. All bacterial cultures were grown at 37°C with agitation at 225 rpm unless otherwise specified.

Purification of BfpB and Western blotting. Wild-type and mutated forms of BfpB were expressed and purified as previously described using the Strep peptide affinity tag (60). BfpB was detected by performing SDS-PAGE. The gels were run according to the manufacturer's instructions (Bio-Rad), and protein was transferred at 21 V for 80 min at 4°C to Immobilon polyvinylidene fluoride membranes (catalog no. IPFL0010; Micropore). Blocking and detection by Western blotting were performed as previously described (65).

Autoaggregation experiments. The functionality of BfpB variants was assessed by the autoaggregation assay using a *bfpB* null strain complemented with plasmids carrying genes encoding each variant; autoaggregation is a phenotype for which functional pili are required (93). The autoaggregation assays were performed as previously described (65, 94), and *bfpB* mutants were qualitatively determined to either autoaggregate or not; only mutants that could autoaggregate were used for labeling experiments.

Iodination of BfpB *in situ* and *in vitro*. The iodination method was modified from a previously published protocol for surface iodination of *V. cholerae* (62). Either *E. coli* XL1-Blue or *E. coli* UMD947 carrying pWS15 was streaked to isolation, and a single colony was picked to inoculate an overnight culture. The following day, cultures were diluted 1:100 and grown to an optical density at 600 nm (OD_{600}) of ~0.5. Expression of BfpB-Strep was induced with 20 μg 100 ml^{-1} of anhydrotetracycline (AHT) for 3 h. Cells were pelleted at 14,000 × *g* for 10 min at 4°C, resuspended, pooled in phosphate-buffered saline (PBS), and washed twice. The cell pellet was weighed and resuspended in PBS to give a concentration of 0.4 g cells ml^{-1}, and approximately 2 to 3 ml of the cell suspension was added to an Iodogen tube (catalog no. 28601; Pierce); as many as two or three tubes were used for each cell suspension to accommodate the volume. The tubes were kept in the dark, and 50 μl of 240 mM sodium iodide was added per 0.1 g of cells (200 μl ml^{-1} cell suspension at 0.4 g ml^{-1}). The cells were incubated rocking on their sides in this solution for 15 min at 30°C in the dark. The contents of each reaction were decanted into a 35-ml Nalgene tube and pooled if multiple Iodogen tubes were needed. The cells were then centrifuged at 14,000 × *g* for 10 min at 4°C, resuspended, and washed in 25 ml PBS. The final cell pellet was frozen at −80°C, and BfpB-Strep was purified as previously described (60). For *in vitro* labeling of purified protein, BfpB-Strep was purified first, and then 3 ml (300 ng μl^{-1}) was incubated in each Iodogen tube with 150 μl of 240 mM NaI. In both cases, purified and labeled BfpB was separated by SDS-PAGE for in-gel digestion and liquid chromatography coupled to tandem mass spectrometry (LC-MS/MS).

In-gel digestion. The in-gel digestion was performed by the Proteomics Core Facility at the University of Maryland, Baltimore. Coomassie blue-stained protein bands were excised, cut into pieces (1 by 1 mm), and dehydrated with methanol for 5 min. The gel pieces were then washed as follows: once for 5 min with 30% methanol−70% water, twice for 10 min with water, and three times for 10 min with 100 mM ammonium bicarbonate (NH_4HCO_3)−30% acetonitrile (vol/vol). Gel pieces were dried in a SpeedVac. Protein disulfide bonds were reduced with 10 mM tris(hydroxypropyl)phosphine in 100 mM NH_4HCO_3 for 1 h at 56°C, followed by alkylation with 55 mM iodoacetamide in 100 mM NH_4HCO_3 for 45 min at room temperature in the dark. The gel pieces were washed with 100 mM NH_4HCO_3 for 15 min and dehydrated with acetonitrile, followed by complete drying in a SpeedVac. Gel pieces were rehydrated in protease solution (15 ng/μl trypsin, GluC, chymotrypsin, or AspN in 50 mM NH_4HCO_3) on ice for 45 min. Excess protease solution was discarded and replaced with 50 mM NH_4HCO_3, and the gel pieces were incubated overnight at 37°C. Digestion buffer was collected and saved. The peptides were extracted once with 50 mM NH_4HCO_3, once with acetonitrile, and twice with 5% formic acid in 50% acetonitrile; each extraction was performed by incubating at 37°C for 15 min with vortexing. All supernatants were combined, dried in a SpeedVac, and desalted using PepClean C_{18} spin columns (catalog no. 89870; Pierce). Desalted peptides were stored at −20°C prior to LC-MS/MS analysis.

LC-MS/MS. Liquid chromatography and tandem mass spectrometry was performed by the Proteomics Core Facility at the University of Maryland, Baltimore. Chromatographic separation of peptides was performed using an Xtreme Simple nano-LC system (Microbiology-Tech Scientific) equipped with a C_{18} reversed-phase column (150 mm by 75 μm) (5-μm particles with 300-Å pores). Mobile phase compositions were as follows: solvent A consisted of 2% acetonitrile and 0.1% formic acid; solvent B consisted of 95% acetonitrile and 0.1% formic acid. Samples were injected in 0.1% formic acid using a Surveyor Autosampler (Thermo Electron). A 40-min LC gradient method from 5 to 40% solvent B at a flow rate of 0.5 μl/min was used to elute the peptides into the mass spectrometer. MS analysis was performed using an LTQ-Orbitrap (Thermo Electron) mass spectrometer equipped with a nanospray ionization source containing an uncoated 10-μm-inner-diameter SilicaTip PicoTip nanospray emitter (New Objective, Inc.). The spray voltage was 1.8 kV, and the heated capillary temperature was 200°C. MS spectra were acquired in the profile mode at 60,000 resolution in the Orbitrap mass analyzer. MS/MS spectra were acquired in the linear ion trap using a top 5 data-dependent acquisition method with dynamic exclusion enabled (repeat count = 1; 180-s exclusion duration). Other mass spectrometric data generation parameters were as follows: collision energy, 35%; full-scan MS mass range, 400 to 1600 *m/z*, minimum signal, 500 counts; isolation width, 3.0 *m/z*.

Peptide and protein identification. MS/MS spectra were searched against a UniProt *E. coli* database concatenated with version 2012.01.01 of the common repository of adventitious protein database (ftp://ftp.thegpm.org/fasta/cRAP). Database searches were conducted by the Proteomics Core Facility at the University of Maryland, Baltimore, using Sorcerer-SEQUEST (Sage-N Research). The database search parameters were as follows: enzyme, trypsin, GluC, chymotrypsin, or AspN; cleavage, full; precursor mass tolerance, 50 ppm; fragment ion tolerance, 0.5 Da; missed cleavages, 2; modifications, Cys carbamidomethylation (+57.02), Met oxidation (+15.99), and Tyr or His iodination (+126.90). The quality of peptide and protein assignments was assessed using PeptideProphet and ProteinProphet. The peptide-level data were filtered using NSP values of

≥0.9. Proteins with probability scores of 1.0 and two or more unique peptides were accepted as confidently identified proteins.

Site-directed cysteine-scanning mutagenesis. Conservative cysteine mutations were made in the primary sequence of *bfpB* in the pWS15 plasmid encoding BfpB-Strep, targeting either serine or threonine codons to minimize alterations of chemical properties. Site-directed mutagenesis was performed using the QuikChange Lightning method (Agilent) and the primers indicated in Table S5 in the supplemental material. All QuikChange primers were purified by high-pressure liquid chromatography (HPLC) and purchased from either IDT or Sigma. Reactions were run as recommended by the manufacturer with the following modifications: 20 to 60 ng of template DNA was used, the annealing temperature was 55°C, and the extension time was 2 min 30 s. PCR products were digested with DpnI and transformed into chemically competent *E. coli* XL10-Gold (Agilent) according to the manufacturer's instructions. Plasmids were purified (Wizard Plus SV miniprep DNA purification system [catalog no. A1460; Promega, Madison, WI]) and sequenced to confirm the mutation. Once confirmed, the constructs were electroporated into electrocompetent *E. coli* UMD923 and assessed by autoaggregation for complementation of the *bfpB* null phenotype. Plasmids carrying genes encoding BfpB variants that could not complement the UMD923 null *bfpB* mutation were not used for topology analysis.

Solvent accessibility labeling of BfpB-CSM with TMM(PEG)$_{12}$. We modified a previously published method utilizing TMM(PEG)$_{12}$ (catalog no. 22361; Pierce) that determined solvent accessibility of purified protein (95). For our *in vivo* labeling experiments, 100 mg TMM(PEG)$_{12}$ was resuspended in 226 μl of dimethyl sulfoxide (DMSO), resulting in a 125 mM solution, aliquoted, and stored under desiccation at −20°C. For *in vivo* labeling of BfpB-CSM, *E. coli* XL10-Gold strains carrying BfpB-CSM plasmids were streaked from glycerol stocks onto LB agar plates with ampicillin and grown overnight at 37°C. Single colonies were used to inoculate cultures of LB broth with ampicillin, grown overnight with shaking (225 rpm) at 37°C, and diluted 1:50 into 5-ml LB broth with ampicillin. The OD was monitored, and BfpB-CSM expression was induced with AHT (20 μg 100 ml^{-1}) when the OD$_{600}$ reached 0.45 to 0.5. BfpB-CSM proteins were expressed for 3 h and then harvested by centrifugation at 2,000 × *g* for 5 min at 4°C. The cells were washed once in buffer A (100 mM NaCl, 100 mM Tris, 1 mM EDTA [pH 7.0]), centrifuged again, and resuspended in 3 ml buffer A. A 1-ml sample was taken at time zero, and 10 μl of *N*-ethylmaleimide (catalog no. 23030; Pierce) (freshly prepared stock, 105 mM; final concentration, 1 mM) was added to the sample. To the remaining 2-ml bacterial suspension, 2.6 μl of TMM(PEG)$_{12}$ was added to the reaction [final concentration of TMM(PEG)$_{12}$, ~178 μM]. The cells were rotated at 4°C for 2 h and then divided into two 1-ml aliquots; each aliquot received 10 μl of *N*-ethylmaleimide (freshly prepared stock, 105 mM; final concentration, 1 mM) to quench the maleimide reaction. The samples were centrifuged at 2,000 × *g* for 5 min at 4°C, and the cell pellet was stored overnight at −80°C. The next day, cell pellets were resuspended in 25 μl of Laemmli buffer, heated at 95°C for 10 min, separated by SDS-PAGE, and analyzed by Western blotting for the presence of unlabeled and labeled BfpB as indicated by a 2.3-kDa shift in relative mobility (M_r). Four independent replicates of this experiment were performed.

***In vitro* FRET assays.** TAMRA-maleimide (catalog no. 81441-25; AnaSpec) was dissolved in 30 μl of dimethylformamide (DMF) and diluted 1:500 in buffer C (100 mM NaCl, 100 mM Tris, 1 mM EDTA [pH 6.8]). The absorbance at 552 nm was measured and used to calculate the concentration of maleimide-conjugated dye (75,190 M^{-1} cm^{-1}). TAMRA-maleimide was added to purified wild-type and cysteine-mutated BfpB-Strep proteins (0.9 μM) at a 10:1 ratio for 1 h. The reaction was quenched with 100-fold excess *N*-ethylmaleimide (catalog no. 23030; Pierce), and the samples were dialyzed five times for a total of 72 h into buffer C at pH 7.0 at 4°C. The acceptor-only fluorescence was read on a Molecular Devices SpectraMax M2e reader (serial no. DE05539) using UV-transparent 96-well plates (catalog no. 3635; Costar) by exciting at 520 nm with a 530-nm long pass filter and collecting emission from 550 to 650 nm in 10-nm steps. SA-488 (catalog no. 21832; Pierce) was added to both TAMRA-maleimide-labeled and unlabeled BfpB constructs in a 1:1 dye/protein ratio and allowed to incubate for 20 min at 4°C. The sample fluorescence was then read by exciting at 465 nm with a 475-nm long pass filter and collecting emission from 490 to 650 nm in 10-nm steps. FRET efficiency was calculated by the formula where the numerator is the fluorescence intensity of the double-labeled sample, and the denominator is the fluorescence intensity in the donor-only labeled sample. At least three independent labeling experiments were performed for each BfpB-CSM strain. Wild-type, BfpB$_{S41C}$, and BfpB$_{T309C}$ were run with each experiment as internal controls. FRET efficiencies were averaged, and the statistical significance of differences between samples was determined using analysis of variance (ANOVA) in Microsoft Excel.

Although the efficiency of FRET is dependent on distance to the inverse 6th power, estimating true distance using FRET is a difficult proposition. The efficiency of energy transfer is also dependent upon the orientation of the fluorophore dipoles, which cannot be readily controlled or predicted in our system; different labeled residues may have different relative dipole orientations (81–83). However, we can make two conclusions using our FRET system. The first conclusion is that a residue displaying FRET efficiency significantly different from the wild-type BfpB baseline likely indicates an extracellular residue, as periplasmic residues are highly unlikely to permit energy transfer of the donor fluorescence. The second is that since the TAMRA-labeled S553C FRET efficiency is approximately 50%, this value can be approximated as our R_o value (distance at FRET from the donor dye to the acceptor dye is 50% efficient) from which we can predict relative distances. Given the proximity to the SA-488 binding peptide affinity tag, we assume this distance to be approximately $R_o = 25$ Å. We do not rely on distance estimates *per se* to establish residue topology, as the value, on which such estimates are critically dependent, may vary from residue to residue.

Flow cytometry of secretins. To prepare DsbA-Strep and intimin$_{557}$-Strep expression vectors, full-length *dsbA* and *eae* (codons 1 to 557) were amplified from *E. coli* E2348/69 genomic DNA using primers dsbA_Strep Fwd/Rev (Fwd stands for forward, and Rev stands for reverse) and intimin557_Strep_Fwd/Rev (see Table S5 in the supplemental material), which introduced asymmetric BsaI restriction sites on either side of the PCR product. The products were cloned into pCR Zero Blunt (Invitrogen, Grand Island, NY), creating pJAL-S1 and pJAL-S2. The inserts were excised with BsaI and cloned into BsaI-digested pASK-IBA3. The PCR primers were designed so that the short flanking DNA exactly mimicked the sites flanking *bfpB* in pASK-IBA3. The resulting products were verified by restriction digestion and sequencing. The same process was used to clone EPEC *escC*, *V. cholerae* epsD, enterotoxigenic *E. coli* gspD, and *P. aeruginosa* pilQ into pASK-IBA3 using the primers shown in Table S5.

For flow cytometry, glycerol stocks were streaked to isolation and used to inoculate LB with ampicillin. After overnight growth at 37°C with agitation at 225 rpm, fresh 5-ml cultures of LB were inoculated with 50 liters of overnight culture of each strain and grown at 37°C to an OD$_{600}$ of 0.5. Expression was induced with 20 g 100 ml^{-1} AHT for 3 h. Aliquots of 1 ml were taken and centrifuged at maximum speed in a benchtop centrifuge for 1 min to remove the medium. The pellets were resuspended in 100 liters PBS containing a 1:200 dilution of stock SA-488 (1 mg/ml) and incubated at room temperature for 30 min. The cells were fixed with 800 liters of 2% (wt/vol) paraformaldehyde (PFA) and incubated on ice for 30 min. The cells were washed three times with 500 liters of PBS to remove excess SA-488 and PFA, and the cell pellets were resuspended in 500 liters PBS with 10 liters of SYTO 16 (catalog no. S7578; Life Technologies) as a nucleic acid counterstain and incubated at room temperature for 30 min. The cells were washed a final three times and resuspended in 500 liters of PBS.

Ten thousand cells for each strain were analyzed using a BD LSRII flow cytometer (Becton, Dickinson). The geometric mean fluorescence inten-

sities (MFI) and percentage of positive cells were recorded for each sample. The experiments were performed in triplicate.

Rules for defining a topology model of BfpB. We identified potential periplasmic residues in BfpB in two ways: (i) histidine or tyrosine residues iodinated in purified protein but not in BfpB labeled in the OMs of intact cells; and (ii) TAMRA-labeled cysteines, endogenous or engineered point mutants, that did not FRET with the C terminus, which we determined to be extracellular by flow cytometry. In contrast, we classified residues as extracellular if (i) they were histidine or tyrosine residues iodinated in BfpB *in situ* in intact cells or (ii) if a TAMRA-labeled cysteine permitted energy transfer from the C-terminal SA-488 donor in FRET experiments. We classified FRET results as likely extracellular if the fluorescence was significantly different from the wild-type background FRET (8%) by ANOVA. We assigned regions where an even or odd number of transmembrane strands were required to maintain residue assignments from the labeling results. We determined the maximum and likely number of beta strands that could fit into each of these regions based on the number of amino acids between anchor residues.

Next, we were able to refine our topology model using the sequence characteristics from our *a priori* assumptions based on characteristics from solved beta barrels in combination with multiple computer predictions of secondary structure and direct assessment of the primary sequence to assign transmembrane domains. In assessing the primary sequence, we preferentially assigned beta strands with aromatic residues at the hydrophobic-hydrophilic interface and alternating hydrophobic-hydrophilic residues, as these are common themes in beta barrel structures (76, 96). In keeping with common features of OMP beta barrels, for our model, we assumed that most periplasmic turns were short, generally consisting of fewer than 10 amino acids (42, 96), although longer turns were allowed (56), we permitted charged residues in the transmembrane strands but rejected models with multiple charged residues in series (88, 97), and we permitted prolines in the transmembrane strands (48, 49).

SUPPLEMENTAL MATERIAL

Supplemental material for this article may be found at http://mbio.asm.org/lookup/suppl/doi:10.1128/mBio.00322-15/-/DCSupplemental.

Table S1, DOCX file, 0.1 MB.
Table S2, DOCX file, 0.01 MB.
Table S3, DOCX file, 0.02 MB.
Table S4, DOCX file, 0.02 MB.
Table S5, DOCX file, 0.02 MB.
Text S1, DOCX file, 0.04 MB.
Figure S1, TIF file, 1.2 MB.
Figure S2, TIF file, 0.4 MB.
Figure S3, JPG file, 0.04 MB.

ACKNOWLEDGMENTS

We acknowledge Aaron Hess for analyzing the ampicillin consumption assay data and Joseph Gillespie for performing the bioinformatic analysis of the IPS. In addition, we thank Shahista Nisa of the Donnenberg laboratory for providing the EPEC genomic DNA from which *eae* and *dsbA* were amplified. Finally, we thank Patrik Bavoil, Hiroshi Nikaido, and Peter Swaan for helpful discussions of selectively labeling OMPs for topology studies.

This work was supported by National Institutes of Health awards T32 GM008181, T32GM066706, and R01 AI37606.

REFERENCES

1. **Craig L, Pique ME, Tainer JA**. 2004. Type IV pilus structure and bacterial pathogenicity. Nat Rev Microbiol **2:**363–378. http://dx.doi.org/10.1038/nrmicro885.
2. **Pelicic V**. 2008. Type IV pili: *e pluribus unum*? Mol Microbiol **68:**827–837. http://dx.doi.org/10.1111/j.1365-2958.2008.06197.x.
3. **Peabody CR, Chung YJ, Yen MR, Vidal-Ingigliardi D, Pugsley AP, Saier MH**. 2003. Type II protein secretion and its relationship to bacterial type IV pili and archaeal flagella. Microbiology **149:**3051–3072. http://dx.doi.org/10.1099/mic.0.26364-0.
4. **Melville S, Craig L**. 2013. Type IV pili in Gram-positive bacteria. Microbiol Mol Biol Rev **77:**323–341. http://dx.doi.org/10.1128/MMBR.00063-12.
5. **Fröls S, Ajon M, Wagner M, Teichmann D, Zolghadr B, Folea M, Boekema EJ, Driessen AJ, Schleper C, Albers SV**. 2008. UV-inducible cellular aggregation of the hyperthermophilic archaeon *Sulfolobus solfataricus* is mediated by pili formation. Mol Microbiol **70:**938–952. http://dx.doi.org/10.1111/j.1365-2958.2008.06459.x.
6. **Piepenbrink KH, Maldarelli GA, Martinez de la Pena CF, Mulvey GL, Snyder GA, De Masi L, von Rosenvinge EC, Günther S, Armstrong GD, Donnenberg MS, Sundberg EJ**. 2014. Structure of *Clostridium difficile* PilJ exhibits unprecedented divergence from known type IV pilins. J Biol Chem **289:**4334–4345. http://dx.doi.org/10.1074/jbc.M113.534404.
7. **Bradley DE**. 1980. A function of *Pseudomonas aeruginosa* PAO polar pili: twitching motility. Can J Microbiol **26:**146–154.
8. **Farinha MA, Conway BD, Glasier LMG, Ellert NW, Irvin RT, Sherburne R, Paranchych W**. 1994. Alteration of the pilin adhesin of *Pseudomonas aeruginosa* PAO results in normal pilus biogenesis but a loss of adherence to human pneumocyte cells and decreased virulence in mice. Infect Immun **62:**4118–4123.
9. **Schoolnik GK, Fernandez R, Tai JY, Rothbard J, Gotschlich EC**. 1984. Gonococcal pili. Primary structure and receptor binding domain. J Exp Med **159:**1351–1370. http://dx.doi.org/10.1084/jem.159.5.1351.
10. **Faast R, Ogierman MA, Stroeher UH, Manning PA**. 1989. Nucleotide sequence of the structural gene, *tcpA*, for a major pilin subunit of *Vibrio cholerae*. Gene **85:**227–231. http://dx.doi.org/10.1016/0378-1119(89)90486-1.
11. **Girón JA, Ho ASY, Schoolnik GK**. 1991. An inducible bundle-forming pilus of enteropathogenic *Escherichia coli*. Science **254:**710–713. http://dx.doi.org/10.1126/science.1683004.
12. **Kotloff KL, Nataro JP, Blackwelder WC, Nasrin D, Farag TH, Panchalingam S, Wu Y, Sow SO, Sur D, Breiman RF, Faruque AS, Zaidi AK, Saha D, Alonso PL, Tamboura B, Sanogo D, Onwuchekwa U, Manna B, Ramamurthy T, Kanungo S**. 2013. Burden and aetiology of diarrhoeal disease in infants and young children in developing countries (the Global Enteric Multicentre Study, GEMS): a prospective, case-control study. Lancet **382:**209–222. http://dx.doi.org/10.1016/S0140-6736(13)60844-2.
13. **Bieber D, Ramer SW, Wu CY, Murray WJ, Tobe T, Fernandez R, Schoolnik GK**. 1998. Type IV pili, transient bacterial aggregates, and virulence of enteropathogenic *Escherichia coli*. Science **280:**2114–2118.
14. **Scaletsky ICA, Milani SR, Trabulsi LR, Travassos LR**. 1988. Isolation and characterization of the localized adherence factor of enteropathogenic *Escherichia coli*. Infect Immun **56:**2979–2983.
15. **Scaletsky ICA, Silva ML, Trabulsi LR**. 1984. Distinctive patterns of adherence of enteropathogenic *Escherichia coli* to HeLa cells. Infect Immun **45:**534–536.
16. **Stone KD, Zhang H-Z, Carlson LK, Donnenberg MS**. 1996. A cluster of fourteen genes from enteropathogenic *Escherichia coli* is sufficient for the biogenesis of a type IV pilus. Mol Microbiol **20:**325–337. http://dx.doi.org/10.1111/j.1365-2958.1996.tb02620.x.
17. **Sohel I, Puente JL, Ramer SW, Bieber D, Wu C-Y, Schoolnik GK**. 1996. Enteropathogenic *Escherichia coli*: identification of a gene cluster coding for bundle-forming pilus morphogenesis. J Bacteriol **178:**2613–2628.
18. **Hwang J, Bieber D, Ramer SW, Wu CY, Schoolnik GK**. 2003. Structural and topographical studies of the type IV bundle-forming pilus assembly complex of enteropathogenic *Escherichia coli*. J Bacteriol **185:**6695–6701. http://dx.doi.org/10.1128/JB.185.22.6695-6701.2003.
19. **Collins RF, Frye SA, Balasingham S, Ford RC, Tønjum T, Derrick JP**. 2005. Interaction with type IV pili induces structural changes in the bacterial outer membrane secretin PilQ. J Biol Chem **280:**18923–18930. http://dx.doi.org/10.1074/jbc.M411603200.
20. **Ayers M, Sampaleanu LM, Tammam S, Koo J, Harvey H, Howell PL, Burrows LL**. 2009. PilM/N/O/P proteins form an inner membrane complex that affects the stability of the *Pseudomonas aeruginosa* type IV pilus secretin. J Mol Biol **394:**128–142. http://dx.doi.org/10.1016/j.jmb.2009.09.034.
21. **Linderoth NA, Model P, Russel M**. 1996. Essential role of a sodium dodecyl sulfate-resistant protein IV multimer in assembly-export of filamentous phage. J Bacteriol **178:**1962–1970.
22. **Allaoui A, Sansonetti PJ, Parsot C**. 1993. MxiD, an outer membrane protein necessary for the secretion of the *Shigella flexneri* Ipa invasins. Mol Microbiol **7:**59–68. http://dx.doi.org/10.1111/j.1365-2958.1993.tb01097.x.

23. **Hodgkinson JL, Horsley A, Stabat D, Simon M, Johnson S, da Fonseca PC, Morris EP, Wall JS, Lea SM, Blocker AJ.** 2009. Three-dimensional reconstruction of the *Shigella* T3SS transmembrane regions reveals 12-fold symmetry and novel features throughout. Nat Struct Mol Biol **16:** 477–485. http://dx.doi.org/10.1038/nsmb.1599.
24. **Korotkov KV, Gonen T, Hol WG.** 2011. Secretins: dynamic channels for protein transport across membranes. Trends Biochem Sci **36:**433–443. http://dx.doi.org/10.1016/j.tibs.2011.04.002.
25. **Reichow SL, Korotkov KV, Gonen M, Sun J, Delarosa JR, Hol WG, Gonen T.** 2011. The binding of cholera toxin to the periplasmic vestibule of the type II secretion channel. Channels (Austin) **5:** 215–218.
26. **Bitter W, Koster M, Latijnhouwers M, De Cock H, Tommassen J.** 1998. Formation of oligomeric rings by XcpQ and PilQ, which are involved in protein transport across the outer membrane of *Pseudomonas aeruginosa*. Mol Microbiol **27:**209–219.
27. **Nouwen N, Ranson N, Saibil H, Wolpensinger B, Engel A, Ghazi A, Pugsley AP.** 1999. Secretin PulD: association with pilot PulS, structure, and ion-conducting channel formation. Proc Natl Acad Sci U S A **96:** 8173–8177. http://dx.doi.org/10.1073/pnas.96.14.8173.
28. **Collins RF, Ford RC, Kitmitto A, Olsen RO, Tønjum T, Derrick JP.** 2003. Three-dimensional structure of the *Neisseria meningitidis* secretin PilQ determined from negative-stain transmission electron microscopy. J Bacteriol **185:**2611–2617. http://dx.doi.org/10.1128/JB.185.8.2611-2617.2003.
29. **Reichow SL, Korotkov KV, Hol WG, Gonen T.** 2010. Structure of the cholera toxin secretion channel in its closed state. Nat Struct Mol Biol **17:**1226–1232. http://dx.doi.org/10.1038/nsmb.1910.
30. **Tosi T, Estrozi LF, Job V, Guilvout I, Pugsley AP, Schoehn G, Dessen A.** 2014. Structural similarity of secretins from type II and type III secretion systems. Structure **22:**1348–1355. http://dx.doi.org/10.1016/j.str.2014.07.005.
31. **Kowal J, Chami M, Ringler P, Müller SA, Kudryashev M, Castaño-Díez D, Amstutz M, Cornelis GR, Stahlberg H, Engel A.** 2013. Structure of the dodecameric *Yersinia enterocolitica* secretin YscC and its trypsin-resistant core. Structure **21:**2152–2161. http://dx.doi.org/10.1016/j.str.2013.09.012.
32. **Collins RF, Frye SA, Kitmitto A, Ford RC, Tønjum T, Derrick JP.** 2004. Structure of the *Neisseria meningitidis* outer membrane PilQ secretin complex at 12-A resolution. J Biol Chem **279:**39750–39756. http://dx.doi.org/10.1074/jbc.M405971200.
33. **Siewering K, Jain S, Friedrich C, Webber-Birungi MT, Semchonok DA, Binzen I, Wagner A, Huntley S, Kahnt J, Klingl A, Boekema EJ, Søgaard-Andersen L, van der Does C.** 2014. Peptidoglycan-binding protein TsaP functions in surface assembly of type IV pili. Proc Natl Acad Sci U S A **111:**E953–E961. http://dx.doi.org/10.1073/pnas.1322889111.
34. **Korotkov KV, Pardon E, Steyaert J, Hol WG.** 2009. Crystal structure of the N-terminal domain of the secretin GspD from ETEC determined with the assistance of a nanobody. Structure **17:**255–265. http://dx.doi.org/10.1016/j.str.2008.11.011.
35. **Spreter T, Yip CK, Sanowar S, André I, Kimbrough TG, Vuckovic M, Pfuetzner RA, Deng W, Yu AC, Finlay BB, Baker D, Miller SI, Strynadka NC.** 2009. A conserved structural motif mediates formation of the periplasmic rings in the type III secretion system. Nat Struct Mol Biol **16:**468–476. http://dx.doi.org/10.1038/nsmb.1603.
36. **Tarry M, Jääskeläinen M, Paino A, Tuominen H, Ihalin R, Högbom M.** 2011. The extra-membranous domains of the competence protein HofQ show DNA binding, flexibility and a shared fold with type I KH domains. J Mol Biol **409:** 642–653. http://dx.doi.org/10.1016/j.jmb.2011.04.034.
37. **Frye SA, Assalkhou R, Collins RF, Ford RC, Petersson C, Derrick JP, Tønjum T.** 2006. Topology of the outer-membrane secretin PilQ from *Neisseria meningitidis*. Microbiology **152:**3751–3764. http://dx.doi.org/10.1099/mic.0.2006/000315-0.
38. **Spagnuolo J, Opalka N, Wen WX, Gagic D, Chabaud E, Bellini P, Bennett MD, Norris GE, Darst SA, Russel M, Rakonjac J.** 2010. Identification of the gate regions in the primary structure of the secretin pIV. Mol Microbiol **76:**133–150. http://dx.doi.org/10.1111/j.1365-2958.2010.07085.x.
39. **Chami M, Guilvout I, Gregorini M, Rémigy HW, Müller SA, Valerio M, Engel A, Pugsley AP, Bayan N.** 2005. Structural insights into the secretin PulD and its trypsin-resistant core. J Biol Chem **280:**37732–37741. http://dx.doi.org/10.1074/jbc.M504463200.
40. **Koebnik R, Locher KP, Van Gelder P.** 2000. Structure and function of bacterial outer membrane proteins: barrels in a nutshell. Mol Microbiol **37:**239–253. http://dx.doi.org/10.1046/j.1365-2958.2000.01983.x.
41. **Buchanan SK.** 1999. Beta-barrel proteins from bacterial outer membranes: structure, function and refolding. Curr Opin Struct Biol **9:**455–461.
42. **Wimley WC.** 2003. The versatile beta-barrel membrane protein. Curr Opin Struct Biol **13:**404–411. http://dx.doi.org/10.1016/S0959-440X(03)00099-X.
43. **Murzin AG, Lesk AM, Chothia C.** 1994. Principles determining the structure of beta-sheet barrels in proteins. II. The observed structures. J Mol Biol **236:** 1382–1400. http://dx.doi.org/10.1016/0022-2836(94)90065-5.
44. **Bayan N, Guilvout I, Pugsley AP.** 2006. Secretins take shape. Mol Microbiol **60:**1–4. http://dx.doi.org/10.1111/j.1365-2958.2006.05084.x.
45. **Pautsch A, Vogt J, Model K, Siebold C, Schulz GE.** 1999. Strategy for membrane protein crystallization exemplified with OmpA and OmpX. Proteins **34:**167–172. http://dx.doi.org/10.1002/(SICI)1097-0134(19990201)34:2<167::AID-PROT2>3.0.CO;2-H.
46. **Baslé A, Rummel G, Storici P, Rosenbusch JP, Schirmer T.** 2006. Crystal structure of osmoporin OmpC from *E. coli* at 2.0 Å. J Mol Biol **362:** 933–942. http://dx.doi.org/10.1016/j.jmb.2006.08.002.
47. **Barnard TJ, Dautin N, Lukacik P, Bernstein HD, Buchanan SK.** 2007. Autotransporter structure reveals intra-barrel cleavage followed by conformational changes. Nat Struct Mol Biol **14:**1214–1220. http://dx.doi.org/10.1038/nsmb1322.
48. **Cowan SW, Schirmer T, Rummel G, Steiert M, Ghosh R, Pauptit RA, Jansonius JN, Rosenbusch JP.** 1992. Crystal structures explain functional properties of two *E. coli* porins. Nature **358:**727–733. http://dx.doi.org/10.1038/358727a0.
49. **Buchanan SK.** 1999. Beta-barrel proteins from bacterial outer membranes: structure, function and refolding. Curr Opin Struct Biol **9:**455–461. http://dx.doi.org/10.1016/S0959-440X(99)80064-5.
50. **Buchanan SK, Lukacik P, Grizot S, Ghirlando R, Ali MM, Barnard TJ, Jakes KS, Kienker PK, Esser L.** 2007. Structure of colicin I receptor bound to the R-domain of colicin Ia: implications for protein import. EMBO J **26:**2594–2604. http://dx.doi.org/10.1038/sj.emboj.7601693.
51. **Ferguson AD, Breed J, Diederichs K, Welte W, Coulton JW.** 1998. An internal affinity-tag for purification and crystallization of the siderophore receptor FhuA, integral outer membrane protein from *Escherichia coli* K-12. Protein Sci **7:**1636–1638. http://dx.doi.org/10.1002/pro.5560070719.
52. **Oomen CJ, van Ulsen P, Van Gelder P, Feijen M, Tommassen J, Gros P.** 2004. Structure of the translocator domain of a bacterial autotransporter. EMBO J **23:**1257–1266. http://dx.doi.org/10.1038/sj.emboj.7600148.
53. **Dautin N.** 2010. Serine protease autotransporters of *Enterobacteriaceae* (SPATEs): biogenesis and function. Toxins (Basel) **2:**1179–1206. http://dx.doi.org/10.3390/toxins2061179.
54. **Luo Y, Frey EA, Pfuetzner RA, Creagh AL, Knoechel DG, Haynes CA, Finlay BB, Strynadka NC.** 2000. Crystal structure of enteropathogenic *Escherichia coli* intimin-receptor complex. Nature **405:**1073–1077. http://dx.doi.org/10.1038/35016618.
55. **Oberhettinger P, Schütz M, Leo JC, Heinz N, Berger J, Autenrieth IB, Linke D.** 2012. Intimin and invasin export their C-terminus to the bacterial cell surface using an inverse mechanism compared to classical autotransport. PLoS One **7:**e47069. http://dx.doi.org/10.1371/journal.pone.0047069.
56. **Koronakis V, Sharff A, Koronakis E, Luisi B, Hughes C.** 2000. Crystal structure of the bacterial membrane protein TolC central to multidrug efflux and protein export. Nature **405:**914–919. http://dx.doi.org/10.1038/35016007.
57. **Meng G, Surana NK, St Geme JW, Waksman G.** 2006. Structure of the outer membrane translocator domain of the *Haemophilus influenzae* Hia trimeric autotransporter. EMBO J **25:**2297–2304. http://dx.doi.org/10.1038/sj.emboj.7601132.
58. **Dong C, Beis K, Nesper J, Brunkan AL, Clarke BR, Whitfield C, Naismith JH.** 2006. The structure of Wza, the translocon for group 1 capsular polysaccharides in *Escherichia coli*, identifies a new class of membrane protein. Nature **444:**226–229. http://dx.doi.org/10.1038/nature05267.
59. **Chandran V, Fronzes R, Duquerroy S, Cronin N, Navaza J, Waksman G.** 2009. Structure of the outer membrane complex of a type IV secretion system. Nature **462:**1011–1015. http://dx.doi.org/10.1038/nature08588.
60. **Daniel A, Singh A, Crowther LJ, Fernandes PJ, Schreiber W, Donnen-**

berg MS. 2006. Interaction and localization studies of enteropathogenic *Escherichia coli* type IV bundle-forming pilus outer membrane components. Microbiology **152:**2405–2420. http://dx.doi.org/10.1099/mic.0.28860-0.
61. **Gardiner PR, Finerty JF, Dwyer DM**. 1983. Iodination and identification of surface membrane antigens in procyclic *Trypanosoma rhodesiense*. J Immunol **131:**454–457.
62. **Richardson K, Parker CD**. 1985. Identification and characterization of *Vibrio cholerae* surface proteins by radioiodination. Infect Immun **48:** 87–93.
63. **Schepky AG, Meinhardt G, Austermann S, Adermann K, Schulz-Knappe P, Forssmann WG, Hass R**. 1996. Specific determination of tyrosine-phosphorylated proteins and peptides by differential iodination. J Chromatogr A **743:**273–282. http://dx.doi.org/10.1016/0021-9673(96)00299-3.
64. **Ramer SW, Bieber D, Schoolnik GK**. 1996. BfpB, an outer membrane lipoprotein required for the biogenesis of bundle-forming pili in enteropathogenic *Escherichia coli*. J Bacteriol **178:**6555–6563.
65. **Lieberman JA, Frost NA, Hoppert M, Fernandes PJ, Vogt SL, Raivio TL, Blanpied TA, Donnenberg MS**. 2012. Outer membrane targeting, ultrastructure, and single molecule localization of the enteropathogenic *Escherichia coli* type IV pilus secretin BfpB. J Bacteriol **194:**1646–1658. http://dx.doi.org/10.1128/JB.06330-11.
66. **Bowden GA, Georgiou G**. 1990. Folding and aggregation of beta-lactamase in the periplasmic space of Escherichia coli. J Biol Chem **265:** 16760–16766.
67. **Guilvout I, Hardie KR, Sauvonnet N, Pugsley AP**. 1999. Genetic dissection of the outer membrane secretin PulD: are there distinct domains for multimerization and secretion specificity? J Bacteriol **181:**7212–7220.
68. **Gromiha MM, Ahmad S, Suwa M**. 2005. TMBETA-NET: discrimination and prediction of membrane spanning beta-strands in outer membrane proteins. Nucleic Acids Res **33:**W164–W167. http://dx.doi.org/10.1093/nar/gki367.
69. **Jacoboni I, Martelli PL, Fariselli P, De Pinto V, Casadio R**. 2001. Prediction of the transmembrane regions of beta-barrel membrane proteins with a neural network-based predictor. Protein Sci **10:**779–787. http://dx.doi.org/10.1110/ps.37201.
70. Koebnik R, Braun V. 1993. Insertion derivatives containing segments of up to 16 amino acids identify surface- and periplasm-exposed regions of the FhuA outer membrane receptor of *Escherichia coli* K-12. J Bacteriol **175:**826–839.
71. **Henderson NS, So SS, Martin C, Kulkarni R, Thanassi DG**. 2004. Topology of the outer membrane usher PapC determined by site-directed fluorescence labeling. J Biol Chem **279:**53747–53754. http://dx.doi.org/10.1074/jbc.M409192200.
72. **Huang Y, Smith BS, Chen LX, Baxter RH, Deisenhofer J**. 2009. Insights into pilus assembly and secretion from the structure and functional characterization of usher PapC. Proc Natl Acad Sci U S A **106:**7403–7407. http://dx.doi.org/10.1073/pnas.0902789106.
73. **Remaut H, Tang C, Henderson NS, Pinkner JS, Wang T, Hultgren SJ, Thanassi DG, Waksman G, Li H**. 2008. Fiber formation across the bacterial outer membrane by the chaperone/usher pathway. Cell **133:** 640–652. http://dx.doi.org/10.1016/j.cell.2008.03.033.
74. **Korotkov KV, Delarosa JR, Hol WGJ**. 2013. A dodecameric ring-like structure of the N0 domain of the type II secretin from enterotoxigenic *Escherichia coli*. J Struct Biol **183:**354–362. http://dx.doi.org/10.1016/j.jsb.2013.06.013.
75. **Login FH, Fries M, Wang X, Pickersgill RW, Shevchik VE**. 2010. A 20-residue peptide of the inner membrane protein OutC mediates interaction with two distinct sites of the outer membrane secretin OutD and is essential for the functional type II secretion system in *Erwinia chrysanthemi*. Mol Microbiol **76:**944–955. http://dx.doi.org/10.1111/j.1365-2958.2010.07149.x.
76. **Jarosławski S, Duquesne K, Sturgis JN, Scheuring S**. 2009. High-resolution architecture of the outer membrane of the gram-negative bacteria *Roseobacter denitrificans*. Mol Microbiol **74:**1211–1222. http://dx.doi.org/10.1111/j.1365-2958.2009.06926.x.
77. **Nikaido H**. 2003. Molecular basis of bacterial outer membrane permeability revisited. Microbiol Mol Biol Rev **67:**593–656. http://dx.doi.org/10.1128/MMBR.67.4.593-656.2003.
78. **Schmidt SA, Bieber D, Ramer SW, Hwang J, Wu CY, Schoolnik G**. 2001. Structure-function analysis of BfpB, a secretin-like protein encoded by the bundle-forming-pilus operon of enteropathogenic *Escherichia coli*. J Bacteriol **183:**4848–4859. http://dx.doi.org/10.1128/JB.183.16.4848-4859.2001.
79. **Hendrickson WA, Pähler A, Smith JL, Satow Y, Merritt EA, Phizackerley RP**. 1989. Crystal structure of core streptavidin determined from multiwavelength anomalous diffraction of synchrotron radiation. Proc Natl Acad Sci U S A **86:**2190–2194. http://dx.doi.org/10.1073/pnas.86.7.2190.
80. **Matias VR, Al-Amoudi A, Dubochet J, Beveridge TJ**. 2003. Cryotransmission electron microscopy of frozen-hydrated sections of *Escherichia coli* and *Pseudomonas aeruginosa*. J Bacteriol **185:**6112–6118. http://dx.doi.org/10.1128/JB.185.20.6112-6118.2003.
81. **van der Meer BW, van der Meer DM, Vogel SS**. 2013. Optimizing the orientation factor KAPPA-SQUARED for more accurate FRET measurements, p 63–104. *In* Medintz I, Hildebrandt N (ed), FRET—Förster resonance energy transfer: from theory to applications. Wiley-VCH Verlag GmbH & Co KGaA, Weinheim, Germany.
82. **Loura LM**. 2012. Simple estimation of Förster resonance energy transfer (FRET) orientation factor distribution in membranes. Int J Mol Sci **13:** 15252–15270. http://dx.doi.org/10.3390/ijms131115252.
83. **Iqbal A, Arslan S, Okumus B, Wilson TJ, Giraud G, Norman DG, Ha T, Lilley DM**. 2008. Orientation dependence in fluorescent energy transfer between Cy3 and Cy5 terminally attached to double-stranded nucleic acids. Proc Natl Acad Sci U S A **105:**11176–11181. http://dx.doi.org/10.1073/pnas.0801707105.
84. **Yip CK, Kimbrough TG, Felise HB, Vuckovic M, Thomas NA, Pfuetzner RA, Frey EA, Finlay BB, Miller SI, Strynadka NC**. 2005. Structural characterization of the molecular platform for type III secretion system assembly. Nature **435:**702–707. http://dx.doi.org/10.1038/nature03554.
85. **Daefler S, Guilvout I, Hardie KR, Pugsley AP, Russel M**. 1997. The C-terminal domain of the secretin PulD contains the binding site for its cognate chaperone, PulS, and confers PulS dependence on pIVf1 function. Mol Microbiol **24:**465–475.
86. **Burghout P, van Boxtel R, Van Gelder P, Ringler P, Müller SA, Tommassen J, Koster M**. 2004. Structure and electrophysiological properties of the YscC secretin from the type III secretion system of *Yersinia enterocolitica*. J Bacteriol **186:**4645–4654. http://dx.doi.org/10.1128/JB.186.14.4645-4654.2004.
87. **Koo J, Tang T, Harvey H, Tammam S, Sampaleanu L, Burrows LL, Howell PL**. 2013. Functional mapping of PilF and PilQ in the *Pseudomonas aeruginosa* type IV pilus system. Biochemistry **52:**2914–2923. http://dx.doi.org/10.1021/bi3015345.
88. **Kreusch A, Neubüser A, Schiltz E, Weckesser J, Schulz GE**. 1994. Structure of the membrane channel porin from *Rhodopseudomonas blastica* at 2.0-Å resolution. Protein Sci **3:**58–63. http://dx.doi.org/10.1002/pro.5560030108.
89. **Schiltz E, Kreusch A, Nestel U, Schulz GE**. 1991. Primary structure of porin from Rhodobacter capsulatus. Eur J Biochem **199:**587–594. http://dx.doi.org/10.1111/j.1432-1033.1991.tb16158.x.
90. **Weiss MS, Kreusch A, Schiltz E, Nestel U, Welte W, Weckesser J, Schulz GE**. 1991. The structure of porin from Rhodobacter capsulatus at 1.8 A resolution. FEBS Lett **280:**379–382. http://dx.doi.org/10.1016/0014-5793(91)80336-2.
91. **Vandeputte-Rutten L, Kramer RA, Kroon J, Dekker N, Egmond MR, Gros P**. 2001. Crystal structure of the outer membrane protease OmpT from Escherichia coli suggests a novel catalytic site. EMBO J **20:** 5033–5039. http://dx.doi.org/10.1093/emboj/20.18.5033.
92. **Schreiber W, Stone KD, Strong MA, DeTolla LJ, Jr, Hoppert M, Donnenberg MS**. 2002. BfpU, a soluble protein essential for type IV pilus biogenesis in enteropathogenic *Escherichia coli*. Microbiology **148:** 2507–2518.
93. **Anantha RP, Stone KD, Donnenberg MS**. 2000. Effects of *bfp* mutations on biogenesis of functional enteropathogenic *Escherichia coli* type IV pili. J Bacteriol **182:**2498–2506. http://dx.doi.org/10.1128/JB.182.9.2498-2506.2000.
94. **Crowther LJ, Anantha RP, Donnenberg MS**. 2004. The inner membrane subassembly of the enteropathogenic *Escherichia coli* bundle-forming pilus machine. Mol Microbiol **52:**67–79. http://dx.doi.org/10.1111/j.1365-2958.2003.03963.x.
95. **Vilen H, Hynönen U, Badelt-Lichtblau H, Ilk N, Jääskeläinen P, Torkkeli M, Palva A**. 2009. Surface location of individual residues of SlpA

provides insight into the *Lactobacillus brevis* S-layer. J Bacteriol **191:** 3339–3349. http://dx.doi.org/10.1128/JB.01782-08.

96. **Bishop C, Wimley W.** 2011. Structural plasticity in self-assembling transmembrane β-sheets. Biophys J **101:**828–836. http://dx.doi.org/10.1016/j.bpj.2011.06.059.
97. **Pautsch A, Schulz GE.** 1998. Structure of the outer membrane protein A transmembrane domain. Nat Struct Biol **5:**1013–1017. http://dx.doi.org/10.1038/2983.
98. **Paramasivam N, Habeck M, Linke D.**. 2012. Is the C-terminal insertional signal in Gram-negative bacterial outer membrane proteins species-specific or not? BMC Genomics **13:**510. http://dx.doi.org/10.1186/1471-2164-13-510.